

See discussions, stats, and author profiles for this publication at: <https://www.researchgate.net/publication/231654614>

Tailoring the Structural Motif of AgCo Nanoalloys: Core/Shell versus Janus-like

ARTICLE *in* THE JOURNAL OF PHYSICAL CHEMISTRY C · JANUARY 2010

Impact Factor: 4.77 · DOI: 10.1021/jp909773x

CITATIONS

41

READS

25

2 AUTHORS, INCLUDING:



Francesca Baletto
King's College London
42 PUBLICATIONS 3,359 CITATIONS

[SEE PROFILE](#)

Tailoring the Structural Motif of AgCo Nanoalloys: Core/Shell versus Janus-like

I. Parsina and F. Baletto*

Physics Department, King's College London, WC2R 2LS, London, U.K.

Received: October 12, 2009; Revised Manuscript Received: December 7, 2009

This paper deals with the computational study of the growth of small silver–cobalt clusters, modeled by a semiempirical potential. Both atom-by-atom growth molecular dynamics and simulations of freezing are used to identify formation patterns of silver–cobalt nanoalloys. Different pathways leading to core/shell and bicompartimentalized configurations, reminiscent of Janus geometry, are observed in cobalt-rich and in silver-rich alloys, respectively. The physical origin of the formation of asymmetric structures and their evolution toward core/shell motifs, as well as the opposite process, are discussed.

Introduction

Metallic nanoalloys¹ are one of the most exciting research objects in materials science because their optical, catalytic, and magnetic properties, different from their bulk values, may have numerous immediate technological applications. Because the physical and chemical properties of nanoparticles are a direct consequence of their electronic structure and, thus, of their geometrical configuration, one of the goals of nanoscience is to be able to design clusters of optimal geometry for a given application simply by tuning their size and chemical composition.² Generally speaking, a bimetallic nanoparticle AB can present various chemical orderings, ranging from a mixed to a completely segregated morphology.^{1,3} Mixed alloys can be either random or ordered, as is the case for the L1₀ geometry of AuCu and AuAg alloys,^{4–6} whereas segregated motifs often manifest themselves as a core/shell order where a core of metal A is surrounded by an external B shell,^{7,8} or multishell alloys, where the A and B metallic layers are alternating as A-B-A⁹ or A-B-A-B.¹⁰ In addition, layered or bicompartimentalized patterns are a possibility. The latter has been recently referred to as “Janus” particles, paying patronage to the Roman god with two faces, Janus, known as the custodian of the Universe.^{11,12}

Nanomixtures of metals that are miscible only at the nanoscale are attracting a lot of attention.^{13–19} This is the case for the silver (Ag) and cobalt (Co) system, which belongs to the class of immiscible materials with silver segregation at cobalt interfaces, composed by a ferro- and a nonferromagnetic metal. These nanoalloys are of interest due to an observed giant magneto-resistance effect, which peaks when a low concentration of cobalt cluster is embedded in a silver film.²⁰ Although Co_{core} and Ag_{shell} are appealing due their catalytic applications, as demonstrated in ref 21, Janus-like AgCo clusters have potential due to their magneto-optical features that could be used for many applications, ranging from the switching on/off of their catalytic properties depending on the orientation of the nanoparticle itself to plasmonics use for cancer treatment and integrated circuits.^{22,23} Today, the basic science behind the preparation, as well as the structural characteristic of bicompartimentalized nanoclusters, is poorly understood. Therefore, proposing the circumstances under which we can design asymmetric particles to occur is undoubtedly of interest. In this paper, our aim is to identify,

through molecular dynamics (MD) simulations, the role of size and chemical composition during the formation of AgCo nanoparticles, in order to answer what is the predominant chemical order as a function of cobalt concentration in a size range from 55 up to 600 atoms. Because of the strong tendency of silver to surface segregate on cobalt, a mixed alloy seems to be very unlikely. Moreover, global optimization (GO) results at selected sizes between 34 and 147 have shown clearly the formation of a core/shell motif with a Co_{core}.²⁴ For the purposes of this work, we distinguish two families of segregated structures: the core/shell, including a multionion core/shell structure, found for other silver nanoalloys,⁹ and the Janus motifs. The Janus and Janus-like patterns individuate nanoparticles that exhibit two well-defined subunits, as recently found during melting simulations of AgNi²⁵ and in experiments for AgCu.²⁶ We have considered and compared two possible formation methods: the atom-by-atom deposition of cobalt over a silver seed and the freezing of AgCo nanodroplets of various sizes and composition. We refer to the former method as *inverse deposition* growth because the seed metal (Ag) has a strong tendency to surface segregate on the deposited metal (Co). The inverse deposition could lead to qualitatively different results from the direct deposition.⁹ Recently, it has been shown that the direct deposition of silver over cobalt results in the formation of a core/shell shape and, in particular, the anti-Mackay icosahedron at Ag₉₂Co₅₅, which is the most favorable structure also from an energetic and thermodynamic point of view.²⁴

We find that the inverse deposition of cobalt easily produces asymmetric structures, namely, up to 15% at small sizes and up to 40–45% at medium-large sizes. This asymmetric structural motif consists of two subunits: one is a pure Ag cluster, often delimited only by (111) facets, and the other is an icosahedral Co core covered by a single monolayer of silver. In the following, these are referred to as *Janus-like* structures because they clearly consist of two distinct “faces”. At any concentration, cobalt prefers to bunch together and grow around subsurface sites. The cobalt unit tries to adopt an icosahedral arrangement, in agreement with the strong tendency of pure cobalt to form Ih at small and intermediate sizes. Anyway, the determination of the best structural motif is far from our analysis: focus on the dynamical formation of a core/shell against Janus-like chemical ordering as a function of cobalt concentration. Moreover, we address the solid–solid transformation path of a motif into the other. In fact, further deposition of cobalt over a

* To whom correspondence should be addressed. E-mail: francesca.baletto@kcl.ac.uk

TABLE 1: Parameters of the Energetic Model for Heteroatomic Interactions for AgCo Systems, Taken from ref 24

alloy	A (eV)	ξ (eV)	$p_{\alpha\beta}$	$q_{\alpha\beta}$	$r_{\alpha\beta}^0$ (Å)	ε_{coh} (eV)
Co–Co	0.1757	1.8430	9.21	2.795	2.500	4.45
Ag–Ag	0.1043	1.1940	10.79	3.190	2.890	2.95
Co–Ag	0.1444	1.4776	10.01	3.085	2.695	

Janus-like system results in well-defined core/shell structures with few defects, depending on the growth condition, whereas the addition of silver over a perfect core/shell leads to the formation of a Janus-like motif. These findings corroborate the hypothesis that the chemical composition is the driving factor behind specific chemical orderings for AgCo nanoalloys.

The paper is organized into the following sections: section II reports the computational approach, with results presented in section III, and a discussion along with conclusions in section IV.

Computational Method

The interparticle interactions are modeled using a semiempirical many-body potential derived within the second moment approximation to the tight-binding model,²⁷ where the total energy E_{tot} is expressed in terms of the sum over all the atoms i of two terms

$$E_{tot} = \sum_i E_i^b + E_i^r \quad (1)$$

where the repulsive Born–Mayer E_i^r part is

$$E_i^r = \sum_j A_{\alpha\beta} e^{-p_{\alpha\beta} \left(\frac{r_{ij}}{r_{\alpha\beta}^0} - 1 \right)} \quad (2)$$

and the band energy term, E_i^b , could be written as

$$E_i^b = - \sum_j \sqrt{\xi_{\alpha\beta}^2 e^{-2q_{\alpha\beta} \left(\frac{r_{ij}}{r_{\alpha\beta}^0} - 1 \right)}} \quad (3)$$

In the above equations, the distance between the atomic sites i and j is r_{ij} , while the nearest-neighbor distance is labeled with $r_{\alpha\beta}^0$, where $\alpha = A, B$ and $\beta = A, B$ have been introduced to distinguish between the two chemical species A and B for the atom i and j , respectively. For the homoatomic pair, r_{AA}^0 or r_{BB}^0 coincides with the pure metal nearest-neighbor distance, while for a heteroatomic pair, it is given by the average of the values in the pure metals:

$$r_{AB}^0 = \frac{r_{AA}^0 + r_{BB}^0}{2} \quad (4)$$

Table 1 reports the potential parameters used in our simulations. They are fitted to several bulk experimental values, such as the cohesive energy ε_{coh} , the lattice parameter, and the elastic constants as the bulk modulus, C_{44} , and C' . The heteroatomic interactions are fitted to the solubility energy of an impurity A into B bulk and vice versa. Agreement with higher accuracy level methods, such as density functional calculations, and with experiments has been proved elsewhere.^{8,16}

Two growth modes were investigated: constant temperature with varying size and constant size with temperature variation. The first mode refers to the atom-by-atom growth over an initial seed.^{28,29} After the thermalization of the initial seed for several picoseconds, atoms are deposited one-by-one with a certain deposition rate, τ^G . The incoming adatom moves with a constant velocity toward the cluster from a randomly allocated site around the center of mass of the seed itself. In between two subsequent depositions, constituent atoms of the cluster are free to move according to Newton's equations of motion, and the overall cluster is thermalized at a temperature T via an Andersen thermostat,³⁰ where the velocities of randomly chosen atoms are extracted from the Boltzmann distribution at the desired temperature. It has been shown that this stochastic thermostat can describe realistically both the growth in inert gas aggregation sources,²⁸ where the nanoparticles are thermalized through collisions with inert gas atoms, and the freezing of nanoparticles.³¹ The robustness is ensured by a suitable thermostat frequency, which does not affect the diffusion properties of the system.^{24,28,29}

Here, we have considered the deposition of cobalt atoms over crystallographic (a regular truncated octahedron, TO_{201}) and noncrystallographic (decahedra, $Dh_{75,146}$ and icosahedra, $Ih_{55,147,309}$) silver cores in the temperature range of 450–650 K. Two different τ^G deposition rates were used: one medium, τ_M^G , corresponding to one atom each 2 ns, and one slow, τ_S^G , equal to one atom each 5 ns. In the instance of growth over very small seeds, a slower rate of 1 atom each 49 ns has been considered. Because the results are not qualitatively different, they are not reported in this paper. Our results are averaged over at least four simulations, done for each possible choice of initial morphology, temperature, and deposition rate. In the case of high temperatures, where the nanoalloy has enough kinetic energy to undergo major structural transformations, we have performed 12 simulations at τ_S^G per each initial silver morphology. No qualitative change appears, notwithstanding consideration of additional statistics.

The second formation mode considered, simulation of freezing of a liquid droplet of a given size and chemical composition,³² mimics cluster growth as a liquid droplet up to a given size, followed by solidification. The clusters to be frozen were chosen among growth snapshots obtained by the inverse deposition method, described previously. The temperature is decreased with a given freezing rate τ^F . Two freezing rates were used: one slow $\tau_S^F = 1$ K/ns and one medium $\tau_M^F = 10$ K/ns. The results are averaged over at least five simulations.

Our analysis is based on both energetic and geometrical considerations. The energetic features are examined by monitoring the energy in excess, versus the number of deposited cobalt atoms, $\Delta = \Delta(N_{dep}^{Co})$. Letting $N_{tot} = N_{seed}^{Ag} + N_{dep}^{Co}$ be the total number of atoms in the cluster, the quantity Δ is defined as

$$\Delta = \frac{E_{tot} - E_{bulk}}{N_{tot}^{3/2}} \quad (5)$$

where E_{tot} is the total energy of the cluster and E_{bulk} is the bulk energy given by $N^{Ag}\varepsilon_{Ag}^{Co} + N^{Co}\varepsilon_{Co}^{Co}$, with obvious meaning of the symbols. Values for the cohesive energies of silver and cobalt are reported in Table 1. Local minima in the excess energy suggest a particularly favorable structural motif. On the other hand, because this quantity is very sensitive to structural defects, frequent during a growth process, even small variations in Δ were investigated.

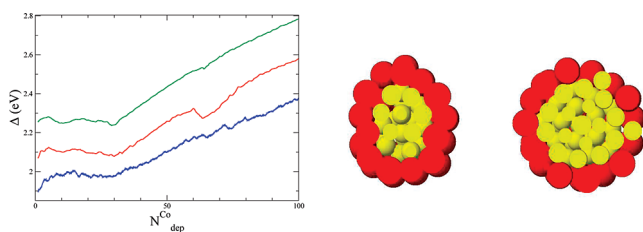


Figure 1. Growth over a Ag-Ih₅₅ seed with a slow deposition rate τ_S^G : excess energy Δ , in eV, as a function of the number of deposited cobalt, $N_{\text{dep}}^{\text{Co}}$, and typical snapshots for $N_{\text{dep}}^{\text{Co}} = 30$ and 65, from growth simulations at 550K. The different color lines in Δ correspond to different temperatures: $T = 450$ K, blue; $T = 550$ K, red; and $T = 650$ K, green line. Δ is averaged over at least 4 simulations for 450 K and 12 for higher temperatures. The yellow color is for cobalt, while red is for silver.

The geometrical characterization is done both by analyzing the first-neighbor environment through the common-neighbor analysis (CNA) as well as by monitoring the evolution of the center of mass (COM) of the silver and cobalt parts versus the whole system. CNA examines the local surroundings of a given pair of nearest neighbors, assigning of a signature represented by three integers (i,j,k): the first integer, i , stands for the number of common nearest neighbors, j relates the number of geometrical bonds between the common neighbors, and the last integer, k , is the number of bonds in the longest chain of bonds.^{33–35} The cluster morphology is identified taking into account the percentage of selected signatures and reference values for pure geometrical models. For example, a pair of nearest neighbors in a five-fold symmetry presents a nonzero value for percentage (5,5,5), P(5,5,5). To distinguish a specific structural motif, more signatures are required: for example, an icosahedron presents a high P(5,5,5) with a high P(4,2,2) and low P(4,2,1) values. The absence of P(5,5,5) and P(4,2,2) shows a crystallographic structure. The policosahedral pattern, as well as an anti-Mackay shell over an Ih, is characterized by a very high value of both P(5,5,5) and P(4,3,3) due to the presence of interpenetrated icosahedra of smaller sizes and the distortion of the tetrahedra forming the cluster, respectively. Other signatures of relevance for this study are (3,2,2), typical of edge atoms in noncrystallographic packing, and (3,1,1), which reveal the presence of (111) facets. A drastic change of CNA signatures can be significant of melting/freezing transition and structural transformation.³²

To detect qualitatively the presence of a bicompartimentalized object, the distances between the center of mass (COM) of silver, $\Delta r_{\text{COM}}^{\text{Ag}}$, and of cobalt, $\Delta r_{\text{COM}}^{\text{Co}}$, units with respect to the COM of the whole structure are monitored. A highly symmetric core-shell structure is expected to have very small $\Delta r_{\text{COM}}^{\text{Ag}}$ and $\Delta r_{\text{COM}}^{\text{Co}}$

because the centers of Ag and Co masses will be ideally coincident. On the other hand, bicompartimentalized structures will present two distinct COMs, $\Delta r_{\text{COM}}^{\text{Ag}}$ and $\Delta r_{\text{COM}}^{\text{Co}}$, at a considerable distance with respect to the cluster radius. Moreover, the initial values of $\Delta r_{\text{COM}}^{\text{Co}}$ give information on where the nucleation starts, while its slope will identify its evolution as a function of Co concentration.

Results

First, we focus our attention on the deposition of cobalt over small silver seeds, the icosahedron Ag-Ih₅₅ and the decahedron Ag-Dh₇₅, with results summarized in Figures 1 and 2, respectively. At low temperatures, the formation of asymmetric structures over the Ih₅₅ is likely at an initial stage of the growth, as identified by an increasing of the excess energy, Δ . After the deposition of ~ 30 Co atoms, the formation of core/shell structures can already be observed. At 550 K, the most significant dip in the quantity Δ occurs after the addition of 60–70 cobalt atoms, corresponding to a rather spherical shape and with an external Ag_{shell}. This is equivalent to the anti-Mackay icosahedron at $N_{\text{tot}} = 127$ atoms, found in the direct growth simulations.²⁴ Further addition of Co atoms makes it difficult for the available Ag atoms to cover the surface of the Co core, and cobalt starts to appear at surface positions. Over Dh₇₅, the cluster undergoes a complete structural transformation toward an icosahedral shape after the deposition of a few cobalt atoms. The change is clearly shown by the CNA signatures, reported in the central panel of Figure 2, where we observe a typical sharp decrease in P(4,2,1) together with a sudden increase of P(5,5,5). At the same time, the rise of the P(3,2,2) and the decline of P(3,1,1) confirm a complete rearrangement of the surface. Further addition of cobalt results in the completion of an icosahedral core around $N_{\text{dep}}^{\text{Co}} \sim 55$ atoms and the formation of an almost complete silver shell on an anti-Mackay stacking around 115–130 atoms, dips in Δ quantity, as happens for the growth over Ih₅₅ and for the direct deposition growth.²⁴

The results for the growth over a medium size noncrystallographic seed are reported in Figure 3, where the top row refers to the growth over a decahedron, Ag-Dh₁₄₆, and the bottom row relates the results for the growth over an icosahedron, Ag-Ih₁₄₇. Both growth snapshots display the formation of Janus-like geometries at the beginning of the growth, up to 30% of cobalt. At sufficiently high temperatures, above 550 K, the growth over Ag-Dh₁₄₆ results in a complete structural transformation toward a core-shell structure, where cobalt is forming an icosahedral core of 147 atoms and silver displaces on an island over an anti-Mackay stacking, reminiscent of the Ag₁₃₂Co₁₄₇ perfect anti-Mackay core/shell. As seen at smaller sizes, the formation of a well-defined icosahedral cobalt unit plus a silver shell is

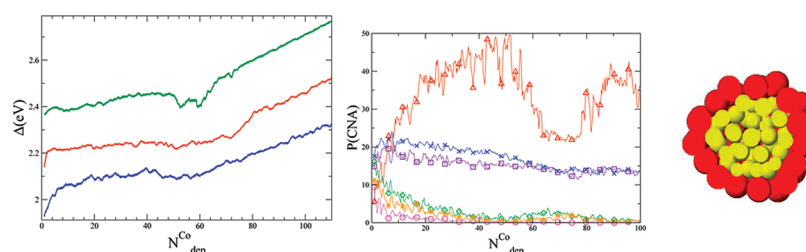


Figure 2. Growth over a Ag-Dh₇₅ decahedral seed with a slow deposition rate τ_S^G : excess energy Δ , in eV, as a function of deposited atoms. Color lines are as in Figure 1. The second panel reports the percentages of typical CNA signatures: P(5,5,5) (red triangles up), P(4,2,1) (magenta circles), P(4,2,2) (orange stars), and P(4,3,3) (violet squares) as well as the signatures P(3,1,1) (green diamonds) and P(3,2,2) (blue crosses) for the description of the (111) facet and its distortion. A complete rearrangement takes place after the intersection of almost all the percentages, indicating that the cluster could be nearly almost melted. The clear drop in P(4,2,1) indicates the transition to an icosahedral motif. The considerably high value of P(5,5,5) suggests the formation of an anti-Mackay shell.

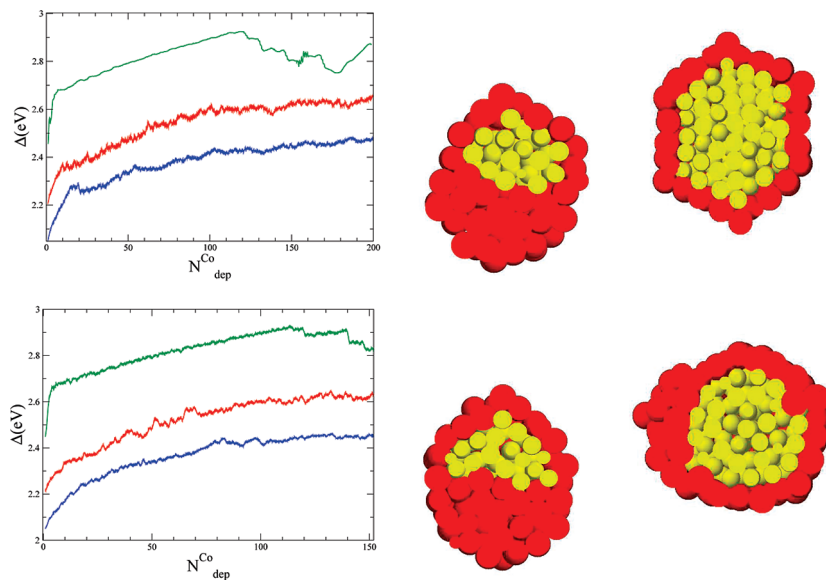


Figure 3. Energy in excess for the growth over medium size silver, as Ag-Dh₁₄₆ (top) and Ag-Ih₁₄₇ (bottom). Color as in Figure 1. Typical snapshots from growth at 650 K are drawn corresponding to $N_{\text{dep}}^{\text{Co}} = 55$ and 147. The initial Janus-like motif naturally evolves toward a core/shell structure for a cobalt concentration higher than 40%.

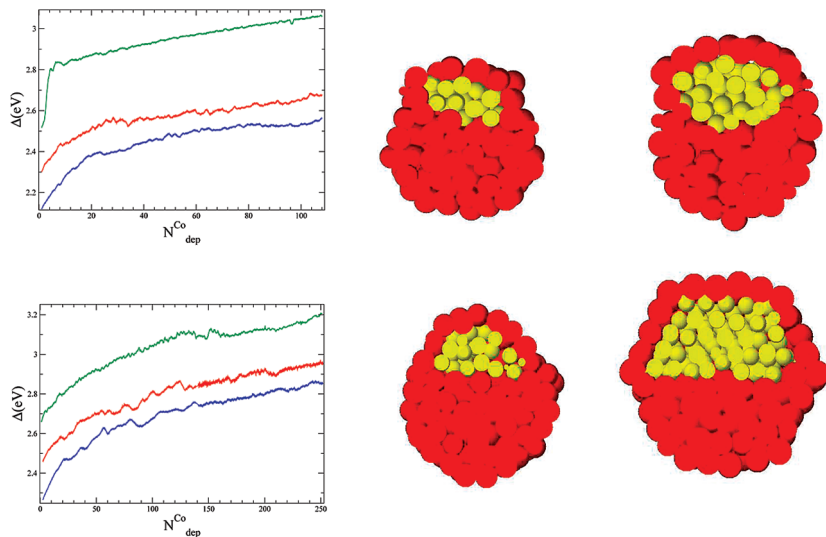


Figure 4. Energy in excess for the growth over Ag-TO₂₀₁ (top row) and Ag-Ih₃₀₉ (bottom). Colors as in Figure 1. Growth snapshots are reported for $N_{\text{dep}}^{\text{Co}} = 34$ and 64 over the Ag-TO₂₀₁ and for $N_{\text{dep}}^{\text{Co}} = 55$ and 139. Here, the formation of Janus-like motifs is very clear up to a concentration of about 45%.

highlighted by dips in the Δ quantity around $N_{\text{dep}}^{\text{Co}} \sim 174$, as shown in Figure 3. At lower temperatures, the nanoalloy presents more nucleation sites for cobalt. Over an Ag-Ih₁₄₇, the cluster grows through similar asymmetric geometries since Co nucleation starts around a subsurface position. The asymmetry is again a Janus-like motif where the pure silver unit still presents an icosahedral shape. This scenario changes after $N_{\text{dep}}^{\text{Co}} \sim 50$, when the whole cluster undergoes a structural transformation, allowing the cobalt to occupy inner positions with the final outcome being a core/shell structure with a silver outer shell. A better example of a complete transformation toward an anti-Mackay silver shell over a cobalt icosahedral core appears only at 650 K around $N_{\text{dep}}^{\text{Co}} \sim 147$, as shown in Figure 3.

The growth over a crystalline Ag-TO₂₀₁ induces structural transformation already after the deposition of 50, at 450 K, and 30, at 550–650 K, cobalt atoms. It is in agreement with the energetic picture that disfavors crystalline morphology at these sizes, for both cobalt and silver.³⁰ The structural transformation from the original crystallographic morphology to a noncrystal-

line one is suggested by a decrease of the P(4,2,1) signature and an increase of the P(5,5,5) and P(4,2,2) pertaining to an icosahedral motif. As an additional confirmation, the surface percentages change in order to decrease P(3,1,1), typical of crystallographic (111) facets, and to increase P(3,2,2), characteristic of edge and under edge atoms in icosahedra. At $T \geq 550$ K, the excess energy presents two dips at $N_{\text{dep}}^{\text{Co}} \sim 34$ and 64, as shown in the top-left panel of Figure 4. The resultant asymmetry motivates the classification of the structures as Janus-like, consisting of a pure silver icosahedron plus a Co_{core}Ag_{shell}, where the cobalt core is a piece of a bigger icosahedron. The pure Ag subunit presents perfect (111) faces, whereas as the conjoined core/shell subcluster, the surface does not present any distinct geometry. At a low temperature of 450 K, more agglomerates of cobalt are formed around different subsurface sites, but the formation of a three-onion shell, observed for other silver alloys,⁹ is hindered by the strong tendency of cobalt and silver to segregate. For the deposition over Ag-Ih₃₀₉, dips in Δ are identified for 650 K growth after the addition of 90 cobalt

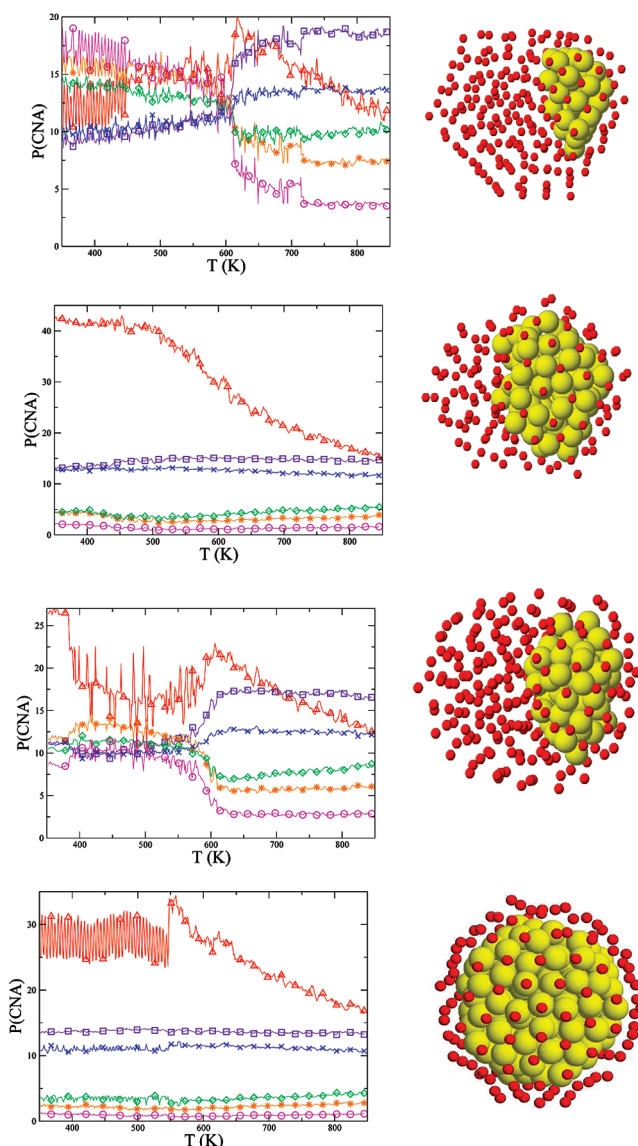


Figure 5. Freezing at different sizes and chemical compositions: CNA analysis averaged over at least five simulations and final snapshot for $\text{Ag}_{201}\text{Co}_{34}$, $\text{Ag}_{147}\text{Co}_{88}$, $\text{Ag}_{201}\text{Co}_{64}$, and $\text{Ag}_{147}\text{Co}_{118}$, from top to bottom. CNA symbols as in Figure 2. The formation of a Janus-like motif is indicated by the increase of $P(5,5,5)$ when the cobalt concentration is less than 40%, otherwise a core/shell is formed, as shown in the bottom row.

atoms and, in particular, when $N_{\text{dep}}^{\text{Co}}$ is between 170–190, as shown in the bottom panel of Figure 4. What we see happening is that the deposited Co atoms take up subsurface positions, then bunch up, leading to the formation of the Janus-like motif, with two well-separated clusters within the Ag seed. The overall structure of the cluster has very distinct (111) facets. The CNA analysis of the cobalt core reveals that it is an icosahedron plus an island over hcp stacking.

Freezing simulations can help us to determine the likeliest configuration at high temperatures as well as to establish the thermal stability of core/shell and Janus-like structures. Nano-droplets at $N_{\text{tot}} = 235$ and 265, taken from growth snapshots at $\text{Ag}_{147}\text{Co}_{88}$ and $\text{Ag}_{147}\text{Co}_{118}$ and at $\text{Ag}_{201}\text{Co}_{34}$ and $\text{Ag}_{201}\text{Co}_{64}$, were considered. We find that the freezing temperature for $N_{\text{tot}} = 265$ is around 650 K and for $N_{\text{tot}} = 235$ around 600 K. The transition is underlined by a sharp change in the CNA percentages, in particular $P(5,5,5)$, as reported in Figure 5. The Janus-like structural motif is easily identified in the final

TABLE 2: Energies, in eV, for the Substitution of a Single Cobalt Impurity in Various Silver Cores with Respect to the Best Site. Except for the Icosahedral Motif, the Subsurface (SS), the One below a Vertex, is the Most Favorable

Ag core	central (C)	subsurface (SS)	vertex (V)	surface (111)
Ih_{55}	0.00	+0.37	+0.80	+0.83
Ih_{147}	0.00	+0.54	+0.92	+0.96
Ih_{309}	0.00	+0.65	+0.98	+1.04
Ag core	central (C)	subsurface (SS)	vertex (V)	surface (111)
Dh_{75}	+0.07	0.00	+0.17	+0.10
Dh_{146}	+0.16	0.00	+0.28	+0.27
Ag core	central (C)	subsurface (SS)	vertex (V)	surface (111)
TO_{201}	+0.17	0.00	+0.21	+0.16
Ag core	central (C)	subsurface (SS)	vertex (V)	surface (100)
				+0.14

snapshot in all the considered cases with a cobalt concentration lower than 40%. On the other hand, at a “magic” size for core/shell AgCo , we found that the freezing preserves the core/shell morphology. Here, we have considered two anti-Mackay silver shells of 72 and 132 atoms over an icosahedral cobalt core of 55 and 147, respectively. These structures could be found in growth simulations. At faster freezing rates, 10 K/ns, the success rate to get a highly symmetric core/shell is around 50%, increasing for slower rates. Moreover, the hysteresis curve in their caloric curves is quite wide: for the $\text{Ag}_{72}\text{Co}_{55}$, the freezing appears almost 50 K lower than the melting, which takes place at 740 K; the $\text{Ag}_{132}\text{Co}_{147}$ solidifies just above 600 K, while its melting temperature is close to 750 K. At a faster freezing rate, the nanoalloy still solidifies in a core/shell motif but the cobalt does not present the icosahedral pattern. Finally, we have considered the core/shell, $\text{Ag}_{146}\text{Co}_{178}$, obtained from the growth over a medium size decahedron. Because it is a cobalt-rich nanoalloy, the cluster solidifies in a core/shell motif, as found in the growth mode. Its freezing temperature is around 650 K, while the melting is above 700 K. The error in the determination of melting/freezing is of ± 15 K. A more accurate analysis of the stability at high temperature and of the melting/freezing transition is under consideration.

The freezing/melting results confirm that, almost independently of the growth method and of cluster size, in silver-rich AgCo nanoalloys, the cobalt tends to agglomerate under a single silver monolayer and repels the silver. In addition, the icosahedral core/shell motif seems to be less and less probable at medium/large sizes and temperatures above 600 K.

Discussion and Conclusion

In all the studied cases, we have found that the growth leads to the formation of two main structural motifs: the expected core/shell and the Janus-like motif. We show that, quite surprisingly, the chemical order of the AgCo nanoalloy can be tailored solely by the chemical composition: in fact, Co-poor compositions are marked by a Janus-like pattern, while an increased Co concentration of 40% or higher facilitates the transformation from a Janus-like to a core/shell motif where the external shell consists of silver atoms. Our results are corroborated by global optimization simulations, reported in Figure 7, and the fact that further deposition of silver atoms over a core/shell particle naturally evolves toward a Janus-like motif, as soon as the cobalt concentration drops under 40%, as reported in Figure 8. The explanation of this result is lying in energetic considerations, such as the energetic gain/loss of

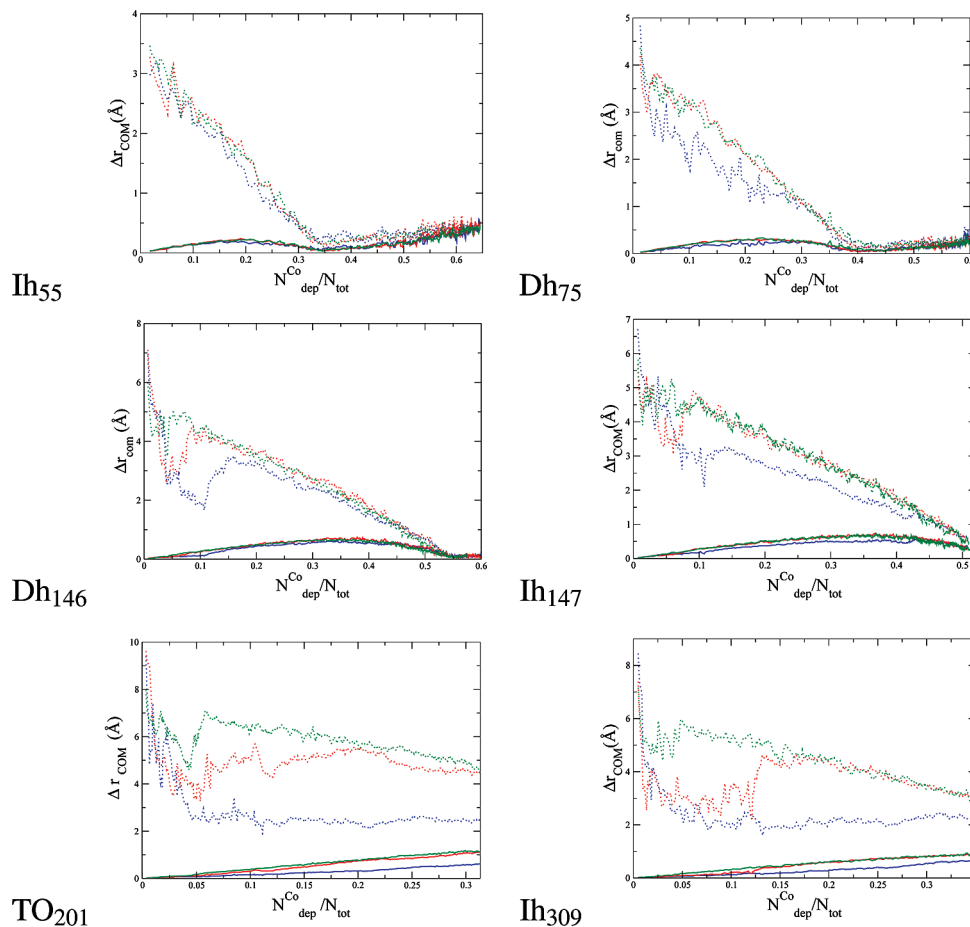


Figure 6. COM analysis: $\Delta r_{\text{COM}}^{\text{Co}}$, in Å, is the distance between the center of mass of the whole cluster and the center of mass of the Co subcluster (dotted line); $\Delta r_{\text{COM}}^{\text{Co}}$, in Å, is the distance of the center of mass of the Co-only subcluster (broken line) for growth at 450 K (blue), 550 K (red), and 650 K (green).

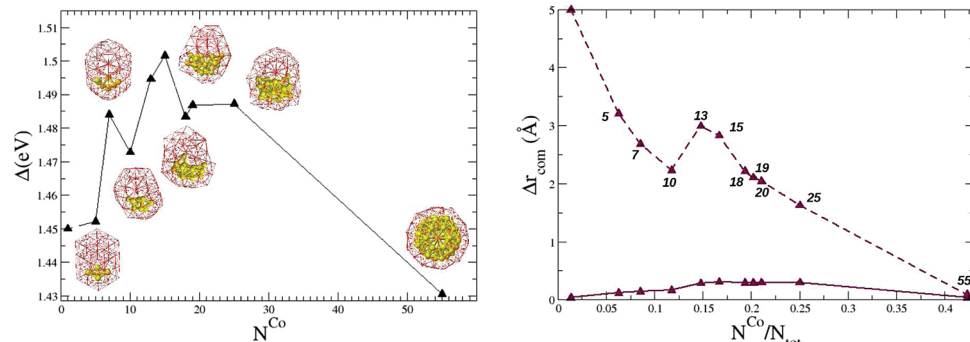


Figure 7. Global optimization results for $\text{Ag}_{75}\text{Co}_x$. Left panel: Δ as a function of the number of cobalt atoms $x = N^{\text{Co}}$. Co atoms are represented by yellow balls, while Ag atoms by the red sticks. Right panel: COM analysis is plotted versus the cobalt concentration. Data points for $\Delta r_{\text{COM}}^{\text{Co}}$ (dashed line) and $\Delta r_{\text{COM}}^{\text{Ag}}$ (full line) are annotated with the corresponding x value. The connecting lines serve as a guide only. The COM analysis is carried out for the best structures obtained.

substituting a silver atom with a more cohesive cobalt and the strong tendency of silver to surface segregate over cobalt. The geometrical analysis of the atomic neighborhood through the first neighbor analysis and the center of mass of the cobalt and silver regions, $\Delta r_{\text{COM}}^{\text{Co}}$ and $\Delta r_{\text{COM}}^{\text{Ag}}$, respectively, as a function of chemical composition, give an estimate of how the nanoalloy evolves as a function of its chemical composition.

The growth patterns could be elucidated by considering the effect of a single cobalt impurity in a silver seed. In fact, independent of the initial silver morphology, the first cobalt atom penetrates the Ag surface easily and remains in a subsurface site, where it acts as a nucleation trap for further incoming Co

atoms. The subsurface sites are the most energetically favorable ones for the implantation of a single cobalt impurity in a silver cluster, as reported in Table 2, except for icosahedral cores, where the central position is energetically preferred by at least 0.4 eV. Nonetheless, the energy gain for putting a cobalt in its best substitution site is between 1 and 1.3 eV for Dh and TO and more than 1.6 eV in the case of icosahedra. Thus, the energetic profile for the substitution impurity supports the hypothesis that the nucleation is likely to start around subsurface positions.

The strong tendency of the considered metals to segregate facilitates the fast nucleation of cobalt atoms into a single

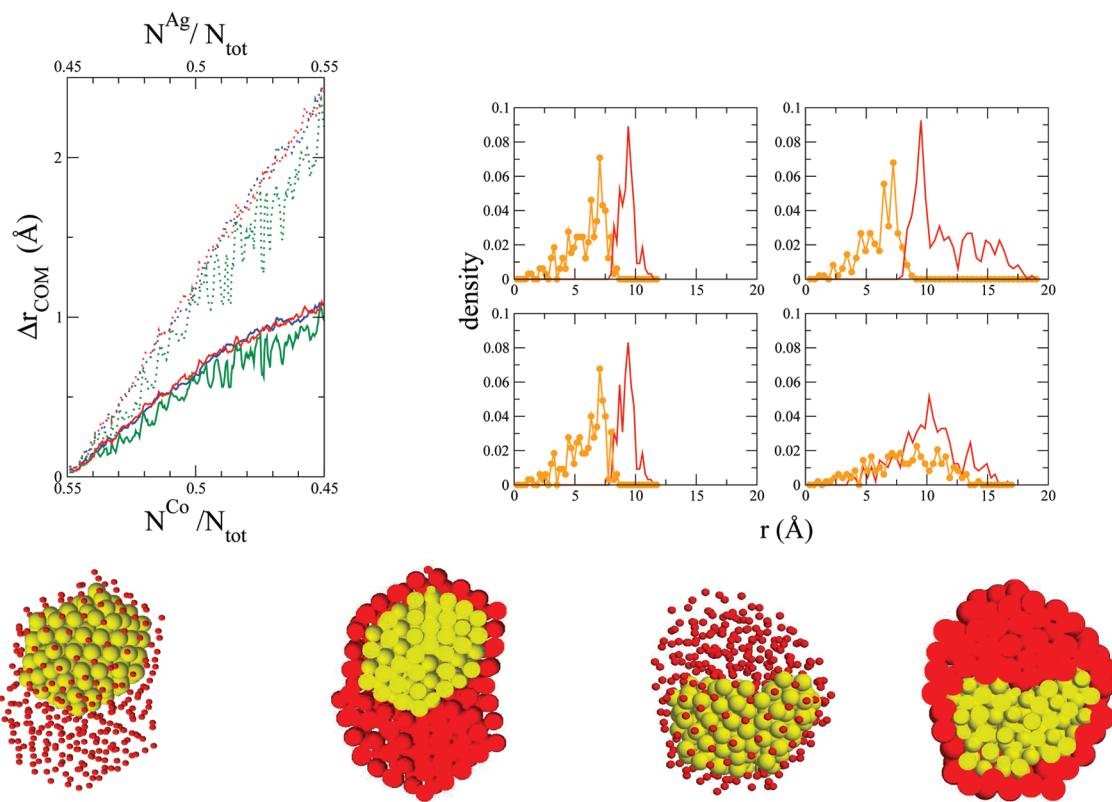


Figure 8. Deposition of silver atoms over a core/shell $\text{Ag}_{146}\text{Co}_{178}$ cluster, which causes the formation of a Janus-like motif. Top row: COM analysis as a function of alloy chemical composition and RDF at the beginning and after the deposition of 163 silver atoms. Typical final snapshot for $\text{Ag}_{309}\text{Co}_{178}$ at 550 K, where the cobalt core is still preserving its icosahedral pattern, and at 650 K, when the cobalt core faces a structural transformation. Averages done over at least four simulations.

agglomerate. In fact, only a few cases, limited by large sizes and low temperatures, are leading to the formation of various subsurface nuclei for cobalt. This scenario has been observed for a cobalt concentration up to 15%, even for small size nanoparticles. The asymmetric growth at a low concentration of cobalt is underlined by the analysis of the evolution of the center of mass of silver (Ag-COM) and cobalt (Co-COM) regions, reported in Figure 6.

The COM analysis provides more details about the formation of the Janus-like motif and how it naturally evolves toward core/shell geometries. The penetration of the first cobalt atom inside the silver cluster, suggested by the energetic scheme, corresponds to the drop in the $\Delta r_{\text{COM}}^{\text{Co}}$, but the subsequent formation of the cobalt nucleus is revealed by the fact that the Co-COM remains distant from the Ag-COM. The softness of the Co-Co interparticle potential drives the so-formed cobalt nucleus to form an icosahedral shape.³⁶ This agglomerate grows, repelling silver atoms, which rearrange over hcp sites on the (111) facets of cobalt, forming an anti-Mackay shell. Namely, values of $\Delta r_{\text{COM}}^{\text{Co}}$ higher than 30% of the initial radius correspond to a Janus-like motif. In that way, we could give approximately the maximum cobalt concentration to get a Janus-like motif. At medium sizes, Ih_{309} and TO_{201} , it is above 45%. Moreover, an estimate of the slope of $\Delta r_{\text{COM}}^{\text{Co}}$ versus the cobalt concentration relates the rate of evolution of the Janus-like structure into a core/shell one. Its intercept with the x axis gives the minimum cobalt concentration to produce a core/shell pattern. Neglecting the results at low temperatures, $T \sim 450$ K, affected by an enhancement of kinetic trappings, a rough estimate shows that this slope is constant in all the considered cases. The minimum cobalt concentration leading to a core/shell motif is roughly given by 0.1 of the initial distance of the first cobalt atom from the whole center of mass.

To test the robustness of our results, we have performed several global optimization runs for Ag_7Co_x , where x ranges from 5 to 55, using parallel excitable walkers (PEW) scheme, as proposed by Ferrando and co-worker.^{37,38} Our results are summarized in Figure 7, where the stability of the structure is monitored by the function Δ , given in eq 5, and the structural motif is analyzed through Δr_{COM} for the obtained global minima for a given cobalt concentration. Clearly, the GO simulations show that the Ag-Co chemical order is tunable by the cobalt concentration in such a way that a Janus-like motif appears in a Ag-rich environment, while a core/shell appears for a concentration approaching 40–45%. Moreover, the structure of the Co unit exhibits clear competition for cobalt to occupy subsurface sites and the tendency to segregate. Already at a very low concentration, cobalt atoms bunch together with a strong preferential occupancy of subsurface sites and respecting five-fold symmetries, however, still failing to form well-defined icosahedral structures even at corresponding magic numbers, such as 13 and 19 atoms. A distinct icosahedral Co core is formed once the transformation toward the core/shell order occurs, resulting in an almost perfect Ih_{55} covered by an external silver shell on an anti-Mackay stacking. From an energetic point of view, the core/shell motif is favored with respect to the Janus-like; nonetheless, the latter remains the best motif for a Co-poor concentration. To further demonstrate that the formation of Janus-like structures is driven by the chemical composition of the nanoalloy, we have considered the deposition of silver atoms over the core/shell obtained at $\text{Ag}_{146}\text{Co}_{178}$. The cobalt core is a Ih_{147} plus a 31-atom island over hcp sites and a silver monolayer shell in an anti-Mackay stacking. The strong tendency of silver to segregate seems to disfavor the formation of a multilayer shell around the cobalt core. In fact, our simulations show Ag preferentially agglomerates on one side

of the core/shell, around one five-fold axis, allowing the formation of a well-defined Janus-like cluster as soon as the cobalt concentration drops below 47%, as shown in Figure 8. In addition to the COM analysis, we have also reported the radial distribution function (RDF), with respect to both Co-COM and Ag-COM at the beginning and after the deposition of 163 silver atoms. Undoubtedly, the cluster grows from a perfect core/shell toward a Janus-like motif, as shown through the RDF, where the atomic density has a different behavior if calculated with respect to the Ag-COM or Co-COM. For the final configuration, we observe that silver atoms form an external shell but the two chemical species became almost homogeneously distributed with respect to the Ag-COM, while the structure is layered if looked from the Co-COM. In addition, we have found that, at high temperatures, the cobalt core is undergoing a structural transformation, as reported in the bottom panels of Figure 8.

To conclude, we have shown that silver–cobalt nanoalloys can present controlled asymmetries even at sizes smaller than 600 atoms. Tailoring asymmetries can be achieved through the growth of cobalt in silver clusters, via the so-called inverse deposition or a freezing technique. At low concentration, cobalt will agglomerate around subsurface sites, leading to the assembly of a Janus-like motif. These Janus-like structures naturally evolve toward a core/shell geometry for a cobalt concentration of more than 40–45% for a medium size nanoparticle. The tendency of cobalt to form an icosahedral unit covered by a monolayer of silver on an anti-Mackay stacking is observed. Further studies on the thermal stability of Janus-like motifs and on their optical/magnetic properties, as well as catalytic, are under investigation.

Acknowledgment. This work is supported by the U.K. research council EPSRC, under Grant No. EP/G003146/1. The authors wish to thank R. Ferrando and A. Mainwood for helpful remarks made in preparing the manuscript.

References and Notes

- (1) Ferrando, R.; Jellinek, J.; Johnston, R. *Chem. Rev.* **2008**, *108*, 845–910.
- (2) Franceschetti, A.; Zunger, A. *Nature* **1999**, *402*, 60.
- (3) Jellinek, J. *Faraday Discussion Meeting 138 on Nanoalloys: From Theory to Application*; Royal Society of Chemistry: London, 2008; p 11.
- (4) Darby, S.; Mortimer-Jones, T. V.; Johnston, R. L.; Roberts, C. *J. Chem. Phys.* **2002**, *116*, 1536.
- (5) Chen, F.; Curley, B. C.; Rossi, G.; Johnston, R. L. *J. Phys. Chem. C* **2007**, *111*, 9157–9165.
- (6) Zhang, M.; Fournier, R. *J. Mol. Struct. (THEOCHEM)* **2006**, *762*, 49–56.
- (7) Hoz, M. D. L.; Tovar, J. M.; Callejas, R.; Balbuena, P. *Mol. Simul.* **2009**, *35*, 785–794.
- (8) Rossi, G.; Rapallo, A.; Mottet, C.; Fortunelli, A.; Baletto, F.; Ferrando, R. *Phys. Rev. Lett.* **2004**, *93*, 105503.
- (9) Baletto, F.; Mottet, C.; Ferrando, R. *Phys. Rev. Lett.* **2003**, *90*, 13504.
- (10) Chen, D.; Wang, W.; Huang, S. *J. Phys. Chem. B* **2006**, *110*, 16193.
- (11) Granick, S.; Jiang, S.; Chen, Q. *Phys. Today* **2009**, *62*, 68.
- (12) Nie, Z.; Li, W.; Seo, M.; Xu, S.; Kumacheva, E. *J. Am. Chem. Soc.* **2006**, *128*, 9408.
- (13) Li, G.; Wang, Q.; Li, D.; et al. *Mater. Chem. Phys.* **2009**, *114*, 746.
- (14) Wang, R.; Dmitrieva, O.; Farle, M.; et al. *J. Phys. Chem. C* **2009**, *113*, 4395.
- (15) Li, G.; Wang, Q.; Li, D.; et al. *Phys. Lett. A* **2008**, *372*, 6764–6769.
- (16) Rives, S.; Catherinot, A.; Dumas-Bouchiat, F.; et al. *Phys. Rev. B* **2008**, *77*, 085407.
- (17) Rivera, M.; Rios-Reyes, C.; Mendoza-Huizar, L. *Appl. Surf. Sci.* **2008**, *255*, 1754–1758.
- (18) Moran-Lopez, J.; Guirado-Lopez, R.; Montejano-Carrizalez, J.; et al. *Curr. Sci.* **2008**, *95*, 1177–1201.
- (19) Janssens, E.; Hoof, T. V.; Veldeman, N.; et al. *Int. J. Mass Spectrom.* **2006**, *252*, 38–46.
- (20) Parent, F.; Tuailon, J.; Stern, L.; Dupuis, V.; Prevel, B.; Perez, A.; Melinon, P.; Guiraud, G.; Morel, R.; Barthelemy, A.; Fert, A. *Phys. Rev. B* **1997**, *55*, 3683.
- (21) Lima, F. H. B.; de Castro, J. F. R.; Ticianelli, E. A. *J. Power Sources* **2006**, *161*, 806.
- (22) Atwater, H. *Sci. Am.* **2007**, *296*, 56.
- (23) Suzuki, D.; Kawaguchi, H. *Colloid Polym. Sci.* **2006**, *284*, 1471–1476.
- (24) Rossi, G.; Schiappelli, G.; Ferrando, R. *J. Comput. Theor. Nanosci.* **2009**, *6*, 841.
- (25) Calvo, F. *Phys. Rev. B* **2008**, *77*, 121406R.
- (26) Cazayous, M.; Langlois, C.; Oikawa, T.; Ricolleau, C.; Sacuto, A. *Microelectron. Eng.* **2007**, *84*, 419.
- (27) Rosato, V.; Guilloue, M.; Legrand, B. *Philos. Mag. A* **1989**, *59*, 321.
- (28) Baletto, F.; Mottet, C.; Ferrando, R. *Surf. Sci.* **2000**, *446*, 31.
- (29) Baletto, F.; Mottet, C.; Ferrando, R. *Phys. Rev. Lett.* **2000**, *84*, 5544.
- (30) Honeycutt, J. D.; Andersen, H. C. *J. Phys. Chem.* **1987**, *91*, 4950.
- (31) Ikeshoji, T.; Torchet, G.; de Feraudy, M. F.; Koga, K. *Phys. Rev. E* **2001**, *63*, 031101.
- (32) Baletto, F.; Mottet, C.; Ferrando, R. *Chem. Phys. Lett.* **2002**, *354*, 82.
- (33) Baletto, F.; Ferrando, R. *Rev. Mod. Phys.* **2005**, *77*, 77.
- (34) Lummen, N.; Krasha, T. *Modell. Simul. Mater. Sci. Eng.* **2007**, *15*, 319.
- (35) Sun, Y. L.; Shen, J. *J. Non-Cryst. Solids* **2009**, *355*, 1557.
- (36) Baletto, F.; Ferrando, R.; Fortunelli, A.; Montalenti, F.; Mottet, C. *J. Chem. Phys.* **2002**, *116*, 3856.
- (37) Rossi, G.; Ferrando, R. *Chem. Phys. Lett.* **2006**, *423*, 17–22.
- (38) Rossi, G.; Ferrando, R. *J. Phys.: Condens. Matter* **2009**, *21*, 084208.

JP909773X